Migdal Ionization as a Probe of Light Dark Matter from Nuclear Transition

Yuanchao Lou,[1,*] Liangliang Su,[2,†] and Lei Wu[1,3,‡]

[1] *Department of Physics and Institute of Theoretical Physics, Nanjing Normal University, Nanjing, 210023, China*
[2] *Institute for Astroparticle Physics, Karlsruhe Institute of Technology, D-76131 Karlsruhe, Germany*
[3] *Nanjing Key Laboratory of Particle Physics and Astrophysics, Nanjing, 210023, China*

Nuclear reactors serve as a key artificial source of light dark matter. Direct detection of reactor-produced dark matter faces substantial obstacles, since quenching effects suppress conventional elastic scattering signals below detector thresholds. We present a new search strategy utilizing the Migdal effect in germanium detectors to probe light dark matter produced via nuclear de-excitation from reactors. Using ON–OFF residual spectra from the TEXONO experiment, we set a new stringent limit on the dark matter and nucleus interaction over the mass range $0.01\,\mathrm{MeV} \leq m_\chi \lesssim 2.6\,\mathrm{MeV}$, which provides a complementary bound to existing cosmological and astrophysical limits.

arXiv:2607.10716v3 [hep-ph] 5 Oct 2026

I. INTRODUCTION

The existence of dark matter (DM) is firmly established by overwhelming gravitational evidence on astrophysical and cosmological scales. However, its fundamental nature at the microscopic level remains one of the most profound mysteries in physics. For decades, the search has been dominated by the Weakly Interacting Massive Particle (WIMP) paradigm (see recent reviews, e.g. [1, 2]). Yet, the continued absence of a confirmed signal in conventional WIMP searches [3–5] has motivated a significant shift in the field towards exploring lighter DM candidates [6–18]. This poses a significant challenge for direct detection, as the resulting nuclear recoils fall far below current detector thresholds, necessitating novel detection strategies (see examples, e.g. [19–32]).

The Migdal effect provides a viable mechanism to circumvent this limitation. During a DM-nucleus scattering event, the sudden acceleration of the nucleus can lead to the ionization or excitation of atomic electrons [33, 34]. This process produces an observable electronic signal, with energy in the eV–keV range, in addition to the tiny nuclear recoil. Later works has revealed its importance for the dark matter direct detection [35–73]. Leveraging the Migdal effect, several searches for sub-GeV dark matter have been performed [74–81]. However, Migdal effect itself remained experimentally unverified in neutron-nucleus scattering until recently, when it was observed in a gaseous detector [82]. This breakthrough has spurred further validation in liquid xenon experiments [83] and other detectors [84, 85].

While direct detection experiments have made significant progress in searching for light dark matter in the galactic halo, nuclear reactors provide a complementary and unique source characterized by an intense high flux of light new particles [86–91]. Unlike the non-relativistic halo dark matter, the dark matter particles produced in nuclear reactors, arising via the decay of light mediators emitted during nuclear de-excitation, $N^* \to N + V(\to \chi\bar{\chi})$, can possess MeV-scale energies since the mediator energy is fixed by the discrete nuclear transition energy, $E_V \simeq \omega_i$. This high-flux, relativistic component offers a distinct opportunity to probe the sub-MeV parameter space that is inaccessible to standard halo searches. However, detecting these reactor-produced particles via standard elastic scattering in semiconductor detectors is hindered by the quenching effect. Since a substantial fraction of the nuclear-recoil energy is dissipated into lattice vibrations, the deposited ionization energy in electron equivalent is typically only a few hundred $\mathrm{eV_{ee}}$. This lies below the threshold of conventional experiments, such as TEXONO germanium detector [92].

In this work, we study Migdal ionization as an observable channel for reactor-produced sub-MeV dark matter in low-threshold germanium detectors. The sudden acceleration of the nucleus can tear off bound electrons, generating an accompanying ionization signal that raises the deposited energy above threshold. The incoming dark matter flux is computed from neutron-capture nuclear de-excitation in ^{238}U and ^{10}B. Using the TEXONO reactor ON–OFF residual spectrum [92], we derive 95% C.L. limits on the reference dark matter–proton cross section $\bar{\sigma}_{\chi p}$ for dark matter masses $0.01\,\mathrm{MeV} < m_\chi < 2.6\,\mathrm{MeV}$. Importantly, since the incident χ flux is generated in the reactor, the limits derived here are independent of the cosmological abundance of χ and do not require χ to constitute all the observed dark matter density. This paper is organized as follows. Section II describes reactor nuclear de-excitation and the resulting dark matter flux. Section III presents the Migdal signal and the resulting TEXONO limits. We conclude in Sec. IV.

II. DARK MATTER PRODUCTION

We consider a kinetically mixed dark photon V [9] coupled to a Dirac fermion dark matter state χ. The relevant

* yuanchao_lou@nnu.edu.cn
† liangliang.su@kit.edu
‡ leiwu@njnu.edu.cn

Lagrangian is

$$\mathcal{L} \supset -\frac{1}{4}V_{\mu\nu}V^{\mu\nu} + \frac{1}{2}m_V^2 V_\mu V^\mu - \frac{\epsilon}{2}V_{\mu\nu}F^{\mu\nu} + g_\chi V_\mu \bar{\chi}\gamma^\mu \chi, \tag{1}$$

where $g_\chi = \sqrt{4\pi\alpha_D}$, m_V is the dark photon mass, which can be generated via the Stueckelberg or dark Higgs mechanism [93–95], and ϵ is the kinetic mixing parameter. After diagonalizing the gauge kinetic terms, V couples to the electromagnetic current with strength ϵe. We focus on the invisible decay regime $m_V > 2m_\chi$ and take $\alpha_D \gg \epsilon^2\alpha$, so that $\mathrm{BR}(V \to \chi\bar{\chi}) \simeq 1$. For the parameter space considered here, the mediator decays promptly near the reactor source.

In the vector-portal scenario, neutron-capture de-excitation provides a line source of vector mediators: an excited nuclear state N^* can de-excite by emitting either a photon or, through kinetic mixing, an on-shell vector mediator V, via $n + N \to N^* \to N + V$, followed by $V \to \chi\bar{\chi}$. The emitted mediator carries energy $E_{V,i} \simeq \omega_i$, where ω_i is the i-th nuclear transition energy, with nuclear recoil corrections negligible at MeV scales. On-shell production is kinematically allowed whenever $m_V < \omega_i$.

For the i-th transition, the mediator production rate at the reactor is

$$\dot{N}_{V,i} = \dot{N}_{\gamma,i}\, r_{E1,i}, \tag{2}$$

where $\dot{N}_{\gamma,i}$ is the ordinary photon emission rate and $r_{E1,i}$ is the dark-vector-to-photon emission ratio. For an E1 transition of energy ω_i [86, 87, 96],

$$r_{E1,i} = \epsilon^2 \left(1 + \frac{m_V^2}{2\omega_i^2}\right)\sqrt{1 - \frac{m_V^2}{\omega_i^2}}\,\Theta(\omega_i - m_V). \tag{3}$$

The ordinary photon emission rate is

$$\dot{N}_{\gamma,i} = N_n \frac{Y_n^{(N)}}{\sum_N Y_n^{(N)}} \frac{I_\gamma^{(N,\omega_i)}}{100}. \tag{4}$$

Here $N_n = 7.8 \times 10^{19}\, P(\mathrm{GW})\ \mathrm{s}^{-1}$ is the total neutron production rate, corresponding to an average fission energy of 200 MeV and 2.5 neutrons per fission [97, 98]. For the TEXONO benchmark with $P = 2.9$ GW, $N_n \simeq 2.3 \times 10^{20}\ \mathrm{s}^{-1}$. $Y_n^{(N)}$ is the neutron-capture yield per fission for isotope N, and $I_\gamma^{(N,\omega_i)}$ is the number of photons of energy ω_i emitted per 100 radiative neutron captures on that isotope [98–100]. For ^{10}B, this photon yield includes the small radiative-capture contribution to $^{10}\mathrm{B}(n,\gamma)^{11}\mathrm{B}$, while the dominant $^{10}\mathrm{B}(n,\alpha)^7\mathrm{Li}$ channel does not contribute to the MeV-scale gamma lines here [100].

The two-body decay $V \to \chi\bar{\chi}$ produces a box-shaped dark matter spectrum with endpoints

$$E_{\chi,i}^{\mathrm{min,max}} = \frac{E_{V,i}}{2} \mp \frac{\sqrt{E_{V,i}^2 - m_V^2}\sqrt{m_V^2 - 4m_\chi^2}}{2m_V}, \tag{5}$$

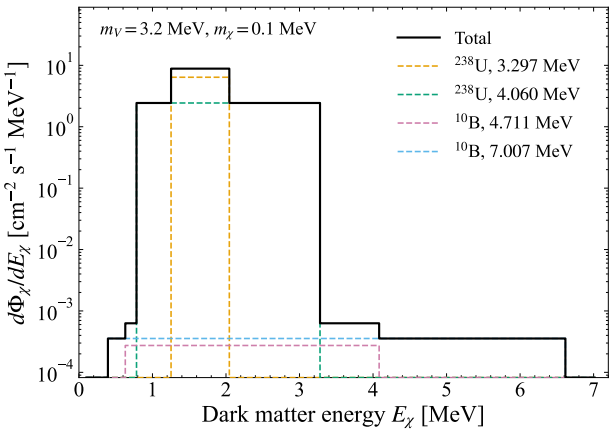


FIG. 1. Reactor dark matter flux from neutron-capture nuclear de-excitation for the benchmark parameters $(m_V, m_\chi) = (3.2, 0.1)$ MeV, $\epsilon = 10^{-5}$, and $\alpha_D = 0.1$. Each transition produces a box-shaped spectrum from $V \to \chi\bar{\chi}$, and the total flux is the sum over the retained lines.

and width $\Delta E_{\chi,i} = E_{\chi,i}^{\max} - E_{\chi,i}^{\min}$. The differential dark matter flux at the detector from the i-th transition is

$$\frac{d\Phi_{\chi,i}}{dE_\chi} = \frac{2\,\dot{N}_{V,i}\,\mathrm{BR}(V \to \chi\bar{\chi})}{4\pi L^2\,\Delta E_{\chi,i}}, \quad E_{\chi,i}^{\min} \le E_\chi \le E_{\chi,i}^{\max}, \tag{6}$$

where $L = 28$ m is the baseline between the Kuo-Sheng reactor core and the TEXONO germanium detector [92],the factor of two accounts for both χ and $\bar{\chi}$, and the total flux is $d\Phi_\chi/dE_\chi = \sum_i d\Phi_{\chi,i}/dE_\chi$.

We use a benchmark set of intense E1 neutron-capture transitions: the 3.297 and 4.060 MeV lines from $^{238}\mathrm{U}(n,\gamma)^{239}\mathrm{U}$, and the 4.711 and 7.007 MeV lines from $^{10}\mathrm{B}(n,\gamma)^{11}\mathrm{B}$. The present source model includes only mediators produced directly in these primary nuclear de-excitation transitions. Secondary production via $\gamma e^- \to V e^-$, as well as contributions from additional capture isotopes or other multipolarities, are not included. A more complete nuclear de-excitation database could modify both the normalization and the spectral shape of the predicted flux. The resulting benchmark dark matter flux is shown in Fig. 1.

III. MIGDAL SIGNAL AND TEXONO LIMITS

We compute the response of a low-threshold germanium detector to the reactor-produced dark matter flux derived in Sec. II. The response is built from elastic nuclear scattering, nuclear recoil quenching, and the single-ionization Migdal contribution. For a single-ionization Migdal process, the total deposited energy is

$$E_{\mathrm{det}} = q_{\mathrm{nr}}(E_{\mathrm{nr}})E_{\mathrm{nr}} + E_{nl} + E_e, \tag{7}$$

where $E_{\rm nr}$ is the nuclear recoil energy, E_{nl} is the binding energy of the shell (n,l), and E_e is the kinetic energy of the emitted electron. Since the detector is sensitive to ionization, only the fraction of the nuclear-recoil energy transferred to electronic excitations contributes to the measured signal. This effect is characterized by the nuclear-recoil quenching factor $q_{\rm nr}(E_{\rm nr})$, which gives the fraction of the recoil energy that is visible in the detector. We evaluate $q_{\rm nr}$ using the Lindhard prescription [101],

$$q_{\rm nr}(E_{\rm nr}) = \frac{k\, g(\varepsilon)}{1 + k\, g(\varepsilon)}, \qquad g(\varepsilon) = 3\varepsilon^{0.15} + 0.7\varepsilon^{0.6} + \varepsilon, \tag{8}$$

with $\varepsilon = 11.5\, Z^{-7/3}(E_{\rm nr}/\mathrm{keV})$ and $k = 0.133\, Z^{2/3} A^{-1/2}$, which gives $k \simeq 0.157$ for germanium.

The corresponding differential Migdal event rate is then obtained by combining the reactor dark matter flux, the nuclear scattering cross section, and the Migdal ionization probability,

$$\begin{aligned}\frac{dR_{\rm Migdal}}{dE_{\rm det}} = N_T \int dE_\chi \frac{d\Phi_\chi}{dE_\chi} \int dE_{\rm nr} \frac{d\sigma_{\chi A}}{dE_{\rm nr}} \\ \times \sum_{n,l} \int dE_e \frac{dp_v(nl \to E_e)}{dE_e} \\ \times \delta(E_{\rm det} - q_{\rm nr}(E_{\rm nr})E_{\rm nr} - E_{nl} - E_e)\,.\end{aligned} \tag{9}$$

Here N_T is the number of germanium target nuclei per unit detector mass, p_v denotes the Migdal ionization probability, and $dp_v(nl \to E_e)/dE_e$ is the differential probability for ionizing an electron from the (n,l) shell with kinetic energy E_e. We compute the Migdal single-ionization probabilities in the isolated-atom approximation. For each occupied germanium orbital from the K through N shells ($1s$, $2s$, $2p$, $3s$, $3p$, $3d$, $4s$, and $4p$), the bound and continuum electron wave functions are generated with cFAC version 1.7.1 [102], a C-based fork of the Flexible Atomic Code [103], and the ionization probability is evaluated from the overlap between the boosted initial electronic state and the final continuum state induced by the sudden nuclear recoil.

Previous studies of the Migdal effect in noble-element targets such as xenon and argon have commonly described the electronic response using atomic ionization probabilities [39, 104], while subsequent studies of semiconductor targets have explicitly included the crystal environment [42, 47]. Here we use isolated-atom Migdal ionization probabilities for germanium and assess this approximation by comparing the relevant atomic and crystal scales. The germanium lattice constant $a \simeq 0.566$ nm corresponds to $p_{\rm lat} \sim \hbar(2\pi/a) \simeq 2.2$ keV$/c$, whereas the M-shell binding energies $E_B \simeq 35$–170 eV imply $p_{\rm atom} \sim \sqrt{2m_e E_B} \simeq 6$–$13$ keV$/c$. With the germanium band gap $E_g \simeq 0.67$ eV [105], these binding energies are also about 50–250 times larger than E_g. These scale comparisons support the isolated-atom treatment for the inner-shell contribution considered here. To remain conservative, we impose $v_N/c \geq 10^{-4}$.

The nuclear scattering cross section entering Eq. (9) is normalized by the reference DM–proton cross section

$$\bar{\sigma}_{\chi p} = \frac{16\pi\alpha\alpha_D\epsilon^2\mu_{\chi p}^2}{(q_0^2 + m_V^2)^2}, \qquad q_0 = \alpha m_e. \tag{10}$$

For a germanium target with $Z = 32$ and nuclear mass m_A, we use

$$\frac{d\sigma_{\chi A}}{dE_{\rm nr}} = \frac{Z^2\bar{\sigma}_{\chi p} F^2(E_{\rm nr})|F_{\rm DM}(q)|^2}{4\mu_{\chi A}^2(E_\chi^2 - m_\chi^2)}\mathcal{K}(E_{\rm nr}), \tag{11}$$

with the Helm form factor $F(E_{\rm nr})$ [106], $q = \sqrt{2m_A E_{\rm nr}}$, the mediator form factor $|F_{\rm DM}(q)|^2 = (q_0^2 + m_V^2)^2/(q^2 + m_V^2)^2$, and the kinematic factor $\mathcal{K}(E_{\rm nr}) = 2m_A E_\chi^2 - E_{\rm nr}(2m_A E_\chi + m_\chi^2 + m_A^2 - m_A E_{\rm nr})$. The Migdal probability is multiplied as an atomic transition factor and does not introduce an additional nuclear form factor.

For the benchmark $(m_V, m_\chi) = (3.2, 0.1)$ MeV, the highest retained de-excitation line, 7.007 MeV, gives $E_\chi^{\rm max} \simeq 6.61$ MeV and hence $E_{\rm nr}^{\rm max} \simeq 1.29$ keV$_{\rm nr}$. After Lindhard quenching, the maximum detected energy from the elastic nuclear recoil is about 0.23 keV$_{\rm ee}$, below the TEXONO threshold. Thus, the elastic NR curve in Fig. 2 ends at the quenched-recoil kinematic endpoint. Migdal ionization adds the electronic energy $(E_{nl}+E_e)$ to the detected signal, allowing events to enter the observable window. For this benchmark, the above-threshold Migdal rate is dominated by the M and L shells, contributing about 85.6% and 13.0%, respectively, while the N and K shells contribute only 1.15% and 0.23%. The M-shell binding energies lie in the range $\sim$ 35–170 eV, and the prominent change of slope near $E_{\rm det} \simeq 1.2$–1.4 keV is associated with the L-shell contribution, dominated by the $2p$ orbital. The K-shell threshold near 11 keV lies in the low-rate tail.

To constrain this channel, we derive constraints from the publicly available TEXONO reactor ON–OFF residual spectrum, defined as the difference between the spectra measured with the reactor operating and shut down, using data from the low-threshold germanium detector at the Kuo-Sheng Reactor Neutrino Laboratory [107]. Since the dark matter flux is produced by the reactor, it is retained in this residual, while reactor-independent backgrounds are reduced by the subtraction. We therefore use the residual spectrum as the observable for the constraint analysis. For each mass point (m_χ, m_V), the bin-averaged signal is

$$S_b(\epsilon, m_V, m_\chi) = \frac{1}{\Delta E_b}\int_{E_b^{\rm min}}^{E_b^{\rm max}} dE_{\rm det}\, \frac{dR_{\rm Migdal}}{dE_{\rm det}}, \tag{12}$$

where $E_b^{\rm min}$ and $E_b^{\rm max}$ are the lower and upper edges of the b-th detector-energy bin and $\Delta E_b = E_b^{\rm max} - E_b^{\rm min}$. We define the Gaussian chi-square as

$$\chi^2(\epsilon, m_V, m_\chi) = \sum_b \frac{[R_b - S_b(\epsilon, m_V, m_\chi)]^2}{\sigma_b^2}, \tag{13}$$

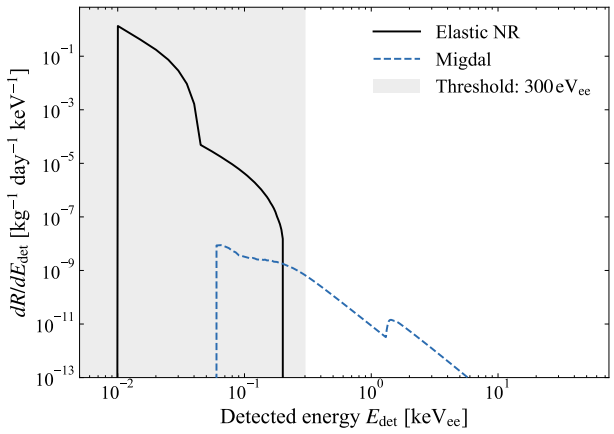


FIG. 2. Differential event rate of reactor-produced light dark matter in the TEXONO germanium detector. The quenched elastic nuclear-recoil contribution lies below the 300 $\mathrm{eV_{ee}}$ analysis threshold for the benchmark shown, while Migdal ionization populates the observable electron-equivalent energy region. The resulting shell-resolved tables for $dP_v(nl \to E_e)/dE_e$ are used in Eq. (9), retaining only kinematically allowed single-ionization events; the successive onset of each orbital's threshold, $E_{\rm det} \gtrsim E_{nl} + q_{\rm nr}E_{\rm nr}$, produces the characteristic changes of slope in the Migdal spectrum shown in Fig. 2. Since the quenched elastic recoil lies below threshold for the reactor-produced MeV-scale flux, the observable signal is dominated by Migdal ionization.

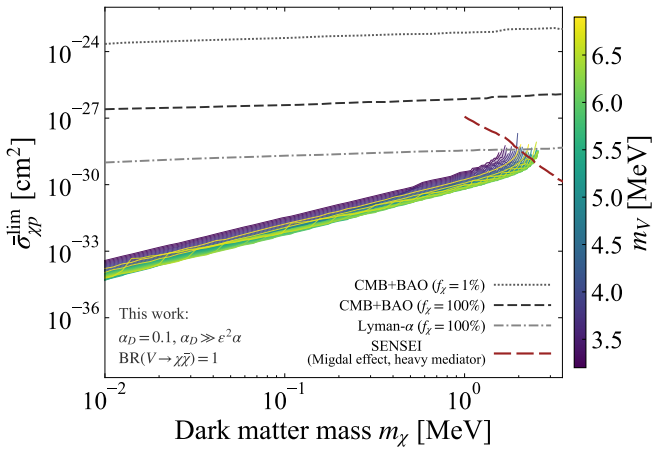


FIG. 3. TEXONO 95% C.L. upper limits on $\bar{\sigma}^{\rm lim}_{\chi p}$ from reactor-produced light dark matter via Migdal ionization in the low-threshold germanium detector, shown as a function of m_χ for m_V in the range 3.2–6.9 MeV (color scale). The limits are obtained in the kinetically mixed dark photon scenario with $\alpha_D = 0.1$ and $\alpha_D \gg \epsilon^2\alpha$, taking the invisible branching ratio to be $\mathrm{BR}(V \to \chi\bar{\chi}) = 1$. Existing constraints are shown for comparison but are not derived within the same theoretical framework. The CMB+BAO and Lyman-α 95% C.L. bounds constrain a velocity-independent DM–proton interaction ($n = 0$) [108], with the assumed interacting dark matter fraction f_χ indicated in the figure. The SENSEI 90% C.L. Migdal (MG) limit assumes Galactic halo dark matter scattering from silicon nuclei through a heavy scalar mediator, with the observable ionization signal generated by the Migdal effect [109]. In contrast to the cosmological bounds, the reactor limits depend on the laboratory-produced $\chi\bar{\chi}$ flux and do not require χ to constitute any specified fraction of the cosmological dark matter abundance.

where R_b and σ_b are the measured ON–OFF residual rate and its uncertainty in the b-th bin. We minimize χ^2 over $\epsilon \geq 0$ and obtain the one-sided 95% C.L. upper limit $\epsilon_{\rm lim}$ from $\Delta\chi^2(\epsilon_{\rm lim}) = 2.71$, with $\Delta\chi^2(\epsilon) = \chi^2(\epsilon) - \chi^2_{\rm min}$. The mediator mass scan covers 3.2 MeV $\leq m_V \leq$ 6.9 MeV, with the lower bound chosen to isolate the neutron-capture de-excitation source from the lower-mass region where Compton-like reactor production can also contribute [86], and the upper bound set below $\omega_{\rm max} =$ 7.007 MeV, where the available de-excitation phase space vanishes.

The resulting 95% C.L. upper limits on $\bar{\sigma}_{\chi p}$ are shown in Fig. 3. For fixed m_χ, larger m_V values are supported mainly by the higher-energy retained transitions, which typically yield more energetic $\chi\bar{\chi}$ pairs. This enhances the Migdal signal in the observable energy window and strengthens the limits over most of the scan range. Close to the endpoint of the highest retained transition, however, the production phase space is suppressed, and the limits weaken as m_V approaches $\omega_{\rm max}$. Theoretically, the mass of dark matter can reach $m_\chi < \omega_{\rm max}/2 \simeq$ 3.50 MeV. However, the present analysis loses sensitivity for $m_\chi \gtrsim$ 2.56 MeV because of the negligible event rate. As m_χ approaches this upper end of the scan, the available phase space and the above-threshold event rate decrease rapidly, producing the upward slope of the limit curves.

For comparison, we show the CMB+BAO and Lyman-α constraints of Ref. [108], together with the SENSEI direct detection limit [109]. These existing bounds are not derived within the same theoretical framework as our reactor constraint. The CMB+BAO and Lyman-α bounds are obtained for a velocity-independent DM–proton interaction ($n = 0$), with the assumed interacting dark matter fraction f_χ indicated in Fig. 3. The SENSEI limit assumes Galactic halo dark matter scattering from silicon nuclei through a heavy scalar mediator, with the observable ionization signal generated by the Migdal effect. By contrast, our reactor limits are obtained in the kinetically mixed dark photon scenario and depend on the laboratory-produced $\chi\bar{\chi}$ flux rather than on the Galactic halo or cosmological abundance of χ. Relevant cosmological constraints also include BBN and $N_{\rm eff}$ bounds, which depend on the thermalization, decoupling, and entropy-transfer history of the dark sector [110, 111], while freeze-in targets depend on both the production history and the relic abundance assigned to χ [112]. Astrophysical constraints from stellar and supernova cooling depend on the in-medium production, absorption, trapping, and trans-

port of dark-sector states [112, 113]. In particular, when dark self-interactions are strong, the produced states may form a coupled dark fluid rather than free-streaming particles, which can substantially modify the resulting constraints [114].

IV. CONCLUSION

We have studied Migdal ionization as an observable channel for reactor-produced sub-MeV dark matter in low-threshold germanium detectors. The reactor source is provided by neutron-capture nuclear de-excitation, in which excited nuclei can emit on-shell kinetically mixed vector mediators in place of ordinary photons. The mediators subsequently decay invisibly into $\chi\bar{\chi}$, producing dark matter with box-shaped energy spectra.

Using selected E1 transitions from $^{238}\mathrm{U}(n,\gamma)^{239}\mathrm{U}$ and $^{10}\mathrm{B}(n,\gamma)^{11}\mathrm{B}$, we computed the resulting reactor dark matter flux at the TEXONO baseline, and calculated the germanium detector response including elastic nuclear scattering, nuclear recoil quenching, and Migdal ionization. For the benchmark spectra considered here, the nuclear recoil contribution alone remains below the 300 $\mathrm{eV_{ee}}$ analysis threshold, while Migdal ionization adds electronic energy to the detector response and provides the relevant visible channel. From the TEXONO reactor ON–OFF residual spectrum, we derived 95% C.L. upper limits on the reference DM–proton cross section $\bar{\sigma}_{\chi p}$, ranging roughly from 6.7×10^{-35} to 8.0×10^{-33} cm^2, for MeV-scale mediators and dark matter masses 0.01 MeV $< m_\chi <$ 2.6 MeV. These limits rely only on the reactor-produced $\chi\bar{\chi}$ flux and the germanium detector response, and do not assume that χ constitutes the cosmological dark matter abundance.

ACKNOWLEDGMENTS

This work is supported by the NNSFC under Grant No. 12275134 and No. 12335005.

[1] G. Bertone, D. Hooper, and J. Silk, Phys. Rept. **405**, 279 (2005), arXiv:hep-ph/0404175.
[2] M. Battaglieri *et al.*, in *U.S. Cosmic Visions: New Ideas in Dark Matter* (2017) arXiv:1707.04591 [hep-ph].
[3] D. S. Akerib *et al.* (LUX), Phys. Rev. Lett. **118**, 021303 (2017), arXiv:1608.07648 [astro-ph.CO].
[4] E. Aprile *et al.* (XENON), Phys. Rev. Lett. **121**, 111302 (2018), arXiv:1805.12562 [astro-ph.CO].
[5] Y. Meng *et al.* (PandaX-4T), Phys. Rev. Lett. **127**, 261802 (2021), arXiv:2107.13438 [hep-ex].
[6] C. Boehm and P. Fayet, Nucl. Phys. B **683**, 219 (2004), hep-ph/0305261.
[7] M. Pospelov, A. Ritz, and M. B. Voloshin, Phys. Lett. B **662**, 53 (2008), arXiv:0711.4866 [hep-ph].
[8] N. Arkani-Hamed, D. P. Finkbeiner, T. R. Slatyer, and N. Weiner, Phys. Rev. D **79**, 015014 (2009), arXiv:0810.0713 [hep-ph].
[9] B. Holdom, Phys. Lett. B **166**, 196 (1986).
[10] J. Alexander *et al.*, Dark Sectors 2016 Workshop: Community Report (2016), arXiv:1608.08632 [hep-ph].
[11] Y. Hochberg, E. Kuflik, T. Volansky, and J. G. Wacker, Phys. Rev. Lett. **113**, 171301 (2014), arXiv:1402.5143 [hep-ph].
[12] Y. Hochberg, E. Kuflik, H. Murayama, T. Volansky, and J. G. Wacker, Phys. Rev. Lett. **115**, 021301 (2015), arXiv:1411.3727 [hep-ph].
[13] E. Kuflik, M. Perelstein, N. Rey-Le Lorier, and Y.-D. Tsai, Phys. Rev. Lett. **116**, 221302 (2016), arXiv:1512.04545 [hep-ph].
[14] E. Kuflik, M. Perelstein, N. Rey-Le Lorier, and Y.-D. Tsai, JHEP **08**, 078, arXiv:1706.05381 [hep-ph].
[15] K. Griest and D. Seckel, Phys. Rev. D **43**, 3191 (1991).
[16] R. T. D'Agnolo and J. T. Ruderman, Phys. Rev. Lett. **115**, 061301 (2015), arXiv:1505.07107 [hep-ph].
[17] J. A. Dror, E. Kuflik, and W. H. Ng, Phys. Rev. Lett. **117**, 211801 (2016), arXiv:1607.03110 [hep-ph].
[18] R. T. D'Agnolo, D. Pappadopulo, and J. T. Ruderman, Phys. Rev. Lett. **119**, 061102 (2017), arXiv:1705.08450 [hep-ph].
[19] R. Essig, A. Manalaysay, J. Mardon, P. Sorensen, and T. Volansky, Phys. Rev. Lett. **109**, 021301 (2012), arXiv:1206.2644 [astro-ph.CO].
[20] R. Essig, M. Fernandez-Serra, J. Mardon, A. Soto, T. Volansky, and T.-T. Yu, JHEP **05**, 046, arXiv:1509.01598 [hep-ph].
[21] H. An, M. Pospelov, J. Pradler, and A. Ritz, Phys. Rev. Lett. **120**, 141801 (2018), [Erratum: Phys.Rev.Lett. 121, 259903 (2018)], arXiv:1708.03642 [hep-ph].
[22] S. Knapen, T. Lin, and K. M. Zurek, Phys. Rev. D **96**, 115021 (2017), arXiv:1709.07882 [hep-ph].
[23] T. Bringmann and M. Pospelov, Phys. Rev. Lett. **122**, 171801 (2019), arXiv:1810.10543 [hep-ph].
[24] C. V. Cappiello and J. F. Beacom, Phys. Rev. D **100**, 103011 (2019), [Erratum: Phys.Rev.D 104, 069901 (2021)], arXiv:1906.11283 [hep-ph].
[25] J. Alvey, M. Campos, M. Fairbairn, and T. You, Phys. Rev. Lett. **123**, 261802 (2019), arXiv:1905.05776 [hep-ph].
[26] L. Su, W. Wang, L. Wu, J. M. Yang, and B. Zhu, Phys. Rev. D **102**, 115028 (2020), arXiv:2006.11837 [hep-ph].
[27] S.-F. Ge, J. Liu, Q. Yuan, and N. Zhou, Phys. Rev. Lett. **126**, 091804 (2021), arXiv:2005.09480 [hep-ph].
[28] Y. Kahn and T. Lin, Rept. Prog. Phys. **85**, 066901 (2022), arXiv:2108.03239 [hep-ph].
[29] W. Wang, L. Wu, W.-N. Yang, and B. Zhu, Phys. Rev. D **107**, 073002 (2023), arXiv:2111.04000 [hep-ph].
[30] L. Su, L. Wu, and B. Zhu, Sci. China Phys. Mech. Astron. **67**, 221012 (2024), arXiv:2308.02204 [hep-ph].
[31] K. I. Nagao, T. Naka, and T. Nomura, JCAP **04**, 030, arXiv:2411.10149 [hep-ph].
[32] Z.-L. Liang, L. Su, L. Wu, and B. Zhu, Phys. Rev. Lett. **134**, 071001 (2025), arXiv:2401.11971 [hep-ph].

[33] A. Migdal, Sov. Phys. JETP **9**, 1163 (1939).
[34] A. B. Migdal, J. Phys. USSR **4**, 449 (1941).
[35] J. D. Vergados and H. Ejiri, Phys. Lett. B **606**, 313 (2005), arXiv:hep-ph/0401151.
[36] C. C. Moustakidis, J. D. Vergados, and H. Ejiri, Nucl. Phys. B **727**, 406 (2005), arXiv:hep-ph/0507123.
[37] H. Ejiri, C. C. Moustakidis, and J. D. Vergados, Phys. Lett. B **639**, 218 (2006), arXiv:hep-ph/0510042.
[38] R. Bernabei *et al.*, Int. J. Mod. Phys. A **22**, 3155 (2007), arXiv:0706.1421 [astro-ph].
[39] M. Ibe, W. Nakano, Y. Shoji, and K. Suzuki, JHEP **03**, 194, arXiv:1707.07258 [hep-ph].
[40] M. J. Dolan, F. Kahlhoefer, and C. McCabe, Phys. Rev. Lett. **121**, 101801 (2018), arXiv:1711.09906 [hep-ph].
[41] N. F. Bell, J. B. Dent, J. L. Newstead, S. Sabharwal, and T. J. Weiler, Phys. Rev. D **101**, 015012 (2020), arXiv:1905.00046 [hep-ph].
[42] R. Essig, J. Pradler, M. Sholapurkar, and T.-T. Yu, Phys. Rev. Lett. **124**, 021801 (2020), arXiv:1908.10881 [hep-ph].
[43] D. Baxter, Y. Kahn, and G. Krnjaic, Phys. Rev. D **101**, 076014 (2020), arXiv:1908.00012 [hep-ph].
[44] Z.-L. Liang, L. Zhang, F. Zheng, and P. Zhang, Phys. Rev. D **102**, 043007 (2020), arXiv:1912.13484 [cond-mat.mes-hall].
[45] V. V. Flambaum, L. Su, L. Wu, and B. Zhu, Sci. China Phys. Mech. Astron. **66**, 271011 (2023), arXiv:2012.09751 [hep-ph].
[46] C. P. Liu, C.-P. Wu, H.-C. Chi, and J.-W. Chen, Phys. Rev. D **102**, 121303 (2020), arXiv:2007.10965 [hep-ph].
[47] S. Knapen, J. Kozaczuk, and T. Lin, Phys. Rev. Lett. **127**, 081805 (2021), arXiv:2011.09496 [hep-ph].
[48] Z.-L. Liang, C. Mo, F. Zheng, and P. Zhang, Phys. Rev. D **104**, 056009 (2021), arXiv:2011.13352 [hep-ph].
[49] J. Liao, H. Liu, and D. Marfatia, Phys. Rev. D **104**, 015005 (2021), arXiv:2104.01811 [hep-ph].
[50] J. F. Acevedo, J. Bramante, and A. Goodman, Phys. Rev. D **105**, 023012 (2022), arXiv:2108.10889 [hep-ph].
[51] W. Wang, K.-Y. Wu, L. Wu, and B. Zhu, Nucl. Phys. B **983**, 115907 (2022), arXiv:2112.06492 [hep-ph].
[52] J. Li, L. Su, L. Wu, and B. Zhu, JCAP **04**, 020, arXiv:2210.15474 [hep-ph].
[53] P. Cox, M. J. Dolan, C. McCabe, and H. M. Quiney, Phys. Rev. D **107**, 035032 (2023), arXiv:2208.12222 [hep-ph].
[54] Z.-L. Liang, C. Mo, F. Zheng, and P. Zhang, Phys. Rev. D **106**, 043004 (2022), [Erratum: Phys.Rev.D 106, 109901 (2022)], arXiv:2205.03395 [hep-ph].
[55] C. Blanco, I. Harris, Y. Kahn, B. Lillard, and J. Pérez-Ríos, Phys. Rev. D **106**, 115015 (2022), arXiv:2208.09002 [hep-ph].
[56] G. Tomar, S. Kang, and S. Scopel, Astropart. Phys. **150**, 102851 (2023), arXiv:2210.00199 [hep-ph].
[57] D. Adams, D. Baxter, H. Day, R. Essig, and Y. Kahn, Phys. Rev. D **107**, L041303 (2023), arXiv:2210.04917 [hep-ph].
[58] K. V. Berghaus, A. Esposito, R. Essig, and M. Sholapurkar, JHEP **01**, 023, arXiv:2210.06490 [hep-ph].
[59] Y. Gu, J. Tang, L. Wu, and B. Zhu, Chin. Phys. C **47**, 125105 (2023), arXiv:2309.09740 [hep-ph].
[60] J. Xu *et al.*, Phys. Rev. D **109**, L051101 (2024), arXiv:2307.12952 [hep-ex].
[61] M. Qiao, C. Xia, and Y.-F. Zhou, JCAP **11**, 079, arXiv:2307.12820 [hep-ph].
[62] Y.-F. Li and S.-y. Xia, Nucl. Phys. B **1006**, 116632 (2024), arXiv:2310.05704 [hep-ph].
[63] G. Herrera, JHEP **05**, 288, arXiv:2311.17719 [hep-ph].
[64] V. A. Dzuba, V. V. Flambaum, and I. B. Samsonov, Phys. Rev. D **109**, 115032 (2024), arXiv:2312.10566 [hep-ph].
[65] Y. Kahn and J. Pérez-Ríos, Phys. Rev. D **110**, 092012 (2024), arXiv:2403.08866 [hep-ex].
[66] S. Kang, S. Scopel, and G. Tomar, JCAP **01**, 035, arXiv:2407.16187 [hep-ph].
[67] W. Nakano, JHEP **10**, 130, arXiv:2410.16911 [hep-ph].
[68] T. N. Maity, Phys. Rev. D **111**, 123020 (2025), arXiv:2412.17649 [hep-ph].
[69] A. Esposito and A. Rocchi, Phys. Rev. D **112**, 075034 (2025), arXiv:2505.08864 [hep-ph].
[70] Q. Mai, G. Huai-Ke, and Z. Yu-Feng, Sci. Sin. Phys. Mech. Astro. **55**, 111006 (2025).
[71] K. V. Berghaus, R. Essig, and M. H. McDuffie, The Migdal effect in Semiconductors for the Effective Field Theory of Dark Matter Direct Detection (2026), arXiv:2603.13052 [hep-ph].
[72] F. Kahlhoefer and L. Su, Probing Sub-GeV Dark Matter via Migdal Effect-Induced Electron Excitations (2026), arXiv:2604.26773 [hep-ph].
[73] S. Nellen Mondragón, J. Pradler, and M. Sholapurkar, Adiabatic response in the Migdal Effect (2026), arXiv:2606.14845 [hep-ph].
[74] D. S. Akerib *et al.* (LUX), Phys. Rev. Lett. **122**, 131301 (2019), arXiv:1811.11241 [astro-ph.CO].
[75] Z. Z. Liu *et al.* (CDEX), Phys. Rev. Lett. **123**, 161301 (2019), arXiv:1905.00354 [hep-ex].
[76] E. Aprile *et al.* (XENON), Phys. Rev. Lett. **123**, 241803 (2019), arXiv:1907.12771 [hep-ex].
[77] G. Adhikari *et al.* (COSINE-100), Phys. Rev. D **105**, 042006 (2022), arXiv:2110.05806 [hep-ex].
[78] P. Agnes *et al.* (DarkSide), Phys. Rev. Lett. **130**, 101001 (2023), arXiv:2207.11967 [hep-ex].
[79] E. Armengaud *et al.* (EDELWEISS), Phys. Rev. D **106**, 062004 (2022), arXiv:2203.03993 [astro-ph.GA].
[80] M. F. Albakry *et al.* (SuperCDMS), Phys. Rev. D **107**, 112013 (2023), arXiv:2302.09115 [hep-ex].
[81] D. Huang *et al.* (PandaX), Phys. Rev. Lett. **131**, 191002 (2023), arXiv:2308.01540 [hep-ex].
[82] D. Yi *et al.*, Nature **649**, 580 (2026).
[83] J. Xu, J. Kim, D. Adams, B. G. Lenardo, W. H. Lippincott, and R. Essig, Nuclear Recoil Migdal Effect in Liquid Xenon Dark Matter Experiments (2026), arXiv:2606.03174 [hep-ex].
[84] H. M. Araújo *et al.* (MIGDAL), Astropart. Phys. **151**, 102853 (2023), arXiv:2207.08284 [hep-ex].
[85] K. D. Nakamura, K. Miuchi, S. Kazama, Y. Shoji, M. Ibe, and W. Nakano, PTEP **2021**, 013C01 (2021), arXiv:2009.05939 [physics.ins-det].
[86] Y. Lou and L. Wu, Probing dark photons from nuclear de-excitation in reactor neutrino experiment (2026), arXiv:2606.08487 [hep-ph].
[87] T. Gao and M. Pospelov, Constraints on millicharged particles from nuclear gamma-decays (2025), arXiv:2507.17955 [hep-ph].
[88] J. J. Choi *et al.* (NEON), Phys. Rev. Lett. **134**, 021802 (2025), arXiv:2407.16194 [hep-ex].
[89] S.-F. Ge and I. M. Shoemaker, JHEP **11**, 066, arXiv:1710.10889 [hep-ph].
[90] W. Dai, Y. Gong, G. Gu, L. Su, L. Wang, L. Wu,

Y. Wu, and L. Yang, Hunting for Axions in REactor neutrino COherent scattering Detection Experiment (2025), arXiv:2509.01538 [hep-ph].
[91] Y. Gong, J. Guo, N. Liu, L. Su, and W.-N. Yang, Constraints on Axion-Like Particles with the Silicon Detector at a Nuclear Reactor (2026), arXiv:2601.07448 [hep-ph].
[92] L. Singh *et al.* (TEXONO), Phys. Rev. D **99**, 032009 (2019), arXiv:1808.02719 [hep-ph].
[93] B. Kors and P. Nath, Phys. Lett. B **586**, 366 (2004), arXiv:hep-ph/0402047.
[94] D. Feldman, Z. Liu, and P. Nath, Phys. Rev. D **75**, 115001 (2007), arXiv:hep-ph/0702123.
[95] D. E. Morrissey, D. Poland, and K. M. Zurek, JHEP **07**, 050, arXiv:0904.2567 [hep-ph].
[96] C. Pitrou and M. Pospelov, Phys. Rev. C **102**, 015803 (2020), arXiv:1904.07795 [astro-ph.CO].
[97] N. Schunck, *Nuclear Fission: Theories, Experiments and Applications* (Springer, 2024).
[98] B. Xin *et al.* (TEXONO), Phys. Rev. D **72**, 012006 (2005), arXiv:hep-ex/0502001.
[99] National Nuclear Data Center, Evaluated Nuclear Structure Data File (ENSDF), https://www.nndc.bnl.gov/ensdf/ (2024), accessed: 2024.
[100] S. F. Mughabghab, *Atlas of Neutron Resonances: Resonance Parameters and Thermal Cross Sections, Z = 1–100*, 5th ed. (Elsevier, Amsterdam, 2006).
[101] J. Lindhard, M. Scharff, and H. E. Schiott, Mat. Fys. Medd. Dan. Vid. Selsk. **33**, 1 (1963).
[102] E. Stambulchik, cFAC: a forked version of FAC, https://github.com/fnevgeny/cfac, version 1.7.1.
[103] M. F. Gu, Can. J. Phys. **86**, 675 (2008).
[104] N. F. Bell, J. B. Dent, R. F. Lang, J. L. Newstead, and A. C. Ritter, Physical Review D **105**, 10.1103/physrevd.105.096015 (2022).
[105] C. Ekuma, M. Jarrell, J. Moreno, and D. Bagayoko, Physics Letters A **377**, 2172–2176 (2013).
[106] R. H. Helm, Phys. Rev. **104**, 1466 (1956).
[107] L. Singh *et al.* (TEXONO), Phys. Rev. D **99**, 032009 (2019), arXiv:1808.02719 [hep-ex].
[108] M. A. Buen-Abad, R. Essig, D. McKeen, and Y.-M. Zhong, Phys. Rept. **961**, 1 (2022), arXiv:2107.12377 [astro-ph.CO].
[109] P. Adari *et al.* (SENSEI), Phys. Rev. Lett. **134**, 011804 (2025), arXiv:2312.13342 [astro-ph.CO].
[110] C. Giovanetti, M. Lisanti, H. Liu, and J. T. Ruderman, Phys. Rev. Lett. **129**, 021302 (2022), arXiv:2109.03246 [hep-ph].
[111] S.-F. Ge, J. Sheng, C. Xia, and C.-Y. Xing, Nuclear Production and Analytic Attenuation of Energetic MeV Solar Dark Matter (2024), arXiv:2408.12448 [hep-ph].
[112] J. H. Chang, R. Essig, and A. Reinert, JHEP **03**, 141, arXiv:1911.03389 [hep-ph].
[113] J. H. Chang, R. Essig, and S. D. McDermott, JHEP **09**, 051, arXiv:1803.00993 [hep-ph].
[114] D. F. G. Fiorillo and E. Vitagliano, Phys. Rev. Lett. **133**, 251004 (2024), arXiv:2404.07714 [hep-ph].